Inorg. Chem. **2005**, *44*, 242–250

Synthesis, Structure, and Properties of [Pt(II)(diimine)(dithiolate)] Dyes with 3,3′-, 4,4′-, and 5,5′-Disubstituted Bipyridyl: Applications in Dye-Sensitized Solar Cells

Elaine A. M. Geary,[†] Lesley J. Yellowlees,[†] Lorna A. Jack,[†] Iain D. H. Oswald,[†] Simon Parsons,[†] Narukuni Hirata,[‡] James R. Durrant,[‡] and Neil Robertson*,[†]

School of Chemistry, University of Edinburgh, Joseph Black Building, Kings Buildings, West Mains Road, Edinburgh, U.K., EH9 3JJ, and Centre for Electronic Materials and Devices, Department of Chemistry, Imperial College London, U.K., SW7 2AZ

Received August 30, 2004

A family of [Pt(II)(diimine)(dithiolate)] complexes of general formula [Pt{*X*,*X*′(CO_2R)$_2$-2,2′-bipyridyl}(maleonitriledithiolate)] (where *X* = 3, 4, or 5 and R = H or Et) have been synthesized, spectroscopically and electrochemically characterized, and attached to a TiO_2 substrate to be tested as solar cell sensitizers. A single-crystal X-ray structure showing a large torsion angle between the bipyridyl rings was determined for [Pt{3,3′(CO_2Et)$_2$-2,2′-bipyridyl}(maleonitriledithiolate)]·MeCN. The effect of changing the position of the bipyridyl substituents from 3,3′ to 4,4′ and 5,5′ is discussed with reference to structural and electronic changes seen within the different members of the family of molecules. The first UV/vis/NIR spectroelectrochemical study of complexes of this general formula is discussed. All three complexes (where R = H) were tested as solar cell sensitizers, with the 3,3′-disubstituted bipyridyl complex giving an intermediate dye loading value but superior photovoltaic performance to those of the other two. The performance of this sensitizer is then compared with that of a well-known Ru polypyridyl sensitizer, the ditetrabutylammonium salt of [$RuL_2(NCS)_2$] (L = 2,2′-bipyridyl-4,4′-dicarboxylato), commonly called N719.

Introduction

In the early 1990s a new avenue of solar cell technology was discovered with the advent of the dye-sensitized solar cell (DSSC).[1] In recent times the synthesis of transition-metal dye molecules for use as solar cell sensitizers has received much interest. Dye molecules anchored to the surface of nanocrystalline TiO_2 absorb visible light and in their excited state they inject an electron into the conduction band of the TiO_2. Ruthenium polypyridyl dyes have received much attention due to their outstanding performance as sensitizers in DSSC, reaching efficiencies of up to 11%.[2−4] Other metal-centered dyes have also been used, including complexes of Fe,[5−7] Os,[8] and Re.[9,10] In the past few years, [Pt(II)(diimine)(dithiolate)] compounds have been investigated for their use in solar cells[11−13] as they possess a number of key features that make them of interest as sensitizers. These include an absorption band in the visible region with a relatively large molar extinction coefficient and in some cases, luminescent properties in fluid solution.

The charge-transfer transition in [Pt(II)(diimine)(dithiolate)] dyes has been assigned as a "mixed metal−ligand

* Corresponding author. Fax: +441316504743. Tel: +441316504755. E-mail: neil.robertson@ed.ac.uk

[†] University of Edinburgh.

[‡] Imperial College London.

(1) O'Regan, B.; Graetzel, M. *Nature* **1991**, *353*, 737.
(2) Nazeeruddin, M. K.; Kay, A.; Rodicio, I.; Humphry-Baker, R.; Mueller, E.; Liska, P.; Vlachopoulos, N.; Graetzel, M. *J. Am. Chem. Soc.* **1993**, *115*, 6382.
(3) Bignozzi, C. A.; Argazzi, R.; Kleverlaan, C. J. *Chem. Soc. Rev.* **2000**, *29*, 87.
(4) Nazeeruddin, M. K.; Graetzel, M. *Comp. Coord. Chem. II* **2004**, *9*, 719.
(5) Ferrere, S. *Chem. Mater.* **2000**, *12*, 1083.
(6) Ferrere, S. *Inorg. Chim. Acta* **2002**, *329*, 79.
(7) Ferrere, S.; Gregg, B. A. *J. Am. Chem. Soc.* **1998**, *120*, 843.
(8) Sauve, G.; Cass, M. E.; Doig, S. J.; Lauermann, I.; Pomykal, K.; Lewis, N. S. *J. Phys. Chem. B* **2000**, *104*, 3488.
(9) Asbury, J. B.; Hao, E.; Wang, Y.; Lian, T. *J. Phys. Chem. B* **2000**, *104*, 11957.
(10) Wang, Y.; Asbury, J. B.; Lian, T. *J. Phys. Chem. A* **2000**, *104*, 4291.
(11) Hissler, M.; McGarrah, J. E.; Connick, W. B.; Geiger, D. K.; Cummings, S. D.; Eisenberg, R. *Coord. Chem. Rev.* **2000**, *208*, 115.
(12) Islam, A.; Sugihara, H.; Hara, K.; Singh, L. P.; Katoh, R.; Yanagida, M.; Takahashi, Y.; Murata, S.; Arakawa, H.; Fujihashi, G. *Inorg. Chem.* **2001**, *40*, 5371.
(13) Geary, E. A. M.; Hirata, N.; Clifford, J.; Durrant, J. R.; Parsons, S.; Dawson, A.; Yellowlees, L. J.; Robertson, N. *Dalton Trans.* **2003**, 3757.

10.1021/ic048799t CCC: $30.25
Published on Web 12/24/2004

to ligand" charge transfer (MMLL′CT) involving a HOMO that is a mixture of Pt(d) and dithiolate S(p) and a LUMO that involves a π^* bpy orbital.[11,14] Substituents on the diimine ligand affect the LUMO energy while substituents on the dithiolate ligand affect the HOMO energy and, therefore, the photophysical and electrochemical properties of the molecule. Tuning of these Pt dye compounds by manipulation of both the HOMO and the LUMO energy levels has been shown by several groups.[12,15] This tuning is relevant in these systems, since the electrochemical and photophysical properties of the dye greatly affect the overall performance of the solar cell.

All dyes investigated for DSSC contain a functionality that anchors the dye to the TiO_2 surface. For the majority of dyes this anchor is {4,4′$(CO_2H)_2$-bpy}, where bpy is 2,2′-bipyridyl. We are interested in what effect the position of the carboxylic acid functionality on the bpy has on the photophysical and electrochemical properties of the dye. Previous publications have shown that the LUMO energy can be altered by changing the position of the carboxylic acid on the bpy ring.[13,15] DFT calculations, electrochemistry, spectroelectrochemistry, and EPR on a family of compounds of general formula [Pt{5,5′$(X)_2$-bpy}Cl_2] (X = H, Me, CO_2Me, CO_2Et, NH_2) have shown that the electron density at the 5,5′-positions is significantly greater than the 4,4′-positions.[16] Therefore, it is expected that substituents at the 5,5′-position have more influence on the electronic characteristics of the bpy than substituents at the 4,4′- or 3,3′-positions. We have shown that by moving the COOH groups from the 4,4′- to the 5,5′-positions on the bpy ring, the HOMO−LUMO energy gap of a [Pt(II)(diimine)(dithiolate)] dye is reduced and this results in shifting the absorbance of the dye to longer wavelength.[13] Most currently available solar cell dyes absorb at shorter wavelengths, and longer wavelength dyes are therefore desirable, since they allow us to harness more of the available solar energy.

Maleonitriledithiolate (mnt) was chosen in our study as the common dithiolate for several reasons. Pt(II) compounds containing mnt have been shown to be emissive in fluid solution as well as frozen glass. The oxidation potential of these complexes is much more positive than the minimum +0.2 V required for this liquid electrolyte solar cell. Finally, previous [Pt(II)(diimine)(mnt)] complexes that have been studied have shown a strong absorption in the visible region.[17,18]

Pt coordination complexes containing a 3,3′-disubstituted bpy ligand have previously been reported in other fields, and [Pt{3,3′$(CO_2H)_2$-bpy}$(Cl)_2$] has been investigated as an anticancer agent.[19] However, no study has been reported of a [Pt(II)(diimine)(dithiolate)] complex with a 3,3′-disubstituted bpy ligand, and initial studies on solar cell dyes containing the {3,3′$(CO_2H)_2$-bpy} anchor have been limited to Ru dyes.[20] In this publication we report the synthesis, characterization, and properties of a family of [Pt(II)(diimine)(dithiolate)] dyes where the variation lies in the position of the COOH group on the bpy ring. We include the first report of a Pt dye containing the {3,3′$(CO_2H)_2$-bpy} anchor and the first crystal structure of a 3,3′-disubstituted bpy in a [Pt(bpy)(1,2-dithiolate)] complex. Our aim is to compare the electrochemical and optical properties of dyes with carboxylic acid substituents at the 3,3′-, 4,4′-,and 5,5′-positions and assess their performances in a DSSC.

Experimental Section

1,10-Phenanthroline, {4,4′$(Me)_2$-bpy}, and {5,5′-$(Me)_2$-bpy}, purchased from Sigma-Aldrich and K_2PtCl_4, purchased from Johnson Matthey, were used as received. Na_2(mnt) was prepared as previously reported.[21]

Synthesis of {3,3′$(CO_2H)_2$-bpy}. {3,3′$(CO_2H)_2$-bpy} was synthesized by a previously reported method.[22] The white solid was recrystallized from water. Yield: 56.4%. Anal. Calcd for $C_{12}H_8N_2O_4$: C, 59.0; H, 3.3; N, 11.5. Found: C, 58.5; H, 3.3; N, 11.3.

Synthesis of {3,3′$(CO_2Et)_2$-bpy}. {3,3′$(CO_2Et)_2$-bpy} was synthesized by a previously reported method.[22] The product did not separate out in aqueous solution but was extracted into DCM and dried with $MgSO_4$ and the solvent removed. Yield: 72.9%. Anal. Calcd for $C_{16}H_{16}N_2O_4$: C, 64.0; H, 5.4; N, 9.3. Found: C, 62.2; H, 5.3; N, 9.0.

Synthesis of {4,4′$(CO_2H)_2$-bpy}. {4,4′$(CO_2H)_2$-bpy} was synthesized by a previously reported method.[23] Yield: 36.2%. Anal. Calcd for $C_{12}H_8N_2O_4 \cdot H_2O$: C, 55.0; H, 3.8; N, 10.7. Found: C, 54.8; H, 3.4; N, 10.8.

Synthesis of {4,4′$(CO_2Et)_2$-bpy}. {4,4′$(CO_2Et)_2$-bpy} was synthesized by a previously reported method.[23] Yield: 38.6%. Anal. Calcd for $C_{16}H_{16}N_2O_4$: C, 64.0; H, 5.4; N, 9.3. Found: C, 62.6; H, 5.0; N, 9.0.

Synthesis of {5,5′$(CO_2H)_2$-bpy}. {5,5′$(CO_2H)_2$-bpy} was synthesized by a previously reported method.[23] Yield: 63.2%. Anal. Calcd for $C_{12}H_8N_2O_4 \cdot H_2O$: C, 55.0; H, 3.8; N, 10.7. Found: C, 54.7; H, 3.4; N, 10.6.

Synthesis of {5,5′$(CO_2Et)_2$-bpy}. {5,5′$(CO_2Et)_2$-bpy} was synthesized by a previously reported method.[23] Yield: 46.6%. Anal. Calcd for $C_{16}H_{16}N_2O_4$: C, 64.0; H, 5.4; N, 9.3. Found: C, 63.2; H, 5.3; N, 9.3.

Synthesis of [Pt{3,3′$(CO_2H)_2$-bpy}Cl_2]. {3,3′$(CO_2H)_2$-bpy} (0.40 g, 1.60 mmol) and K_2PtCl_4 (0.57 g, 1.36 mmol) were refluxed in 100 mL of water for 18 h. A bright yellow powder precipitated on cooling. Yield: 94.8%. Anal. Calcd for $C_{12}H_8N_2O_4PtCl_2$: C, 28.3; H, 1.6; N, 5.5. Found: C, 29.5; H, 1.8; N, 5.6.

Synthesis of [Pt{3,3′$(CO_2Et)_2$-bpy}Cl_2]. A suspension of {3,3′$(CO_2Et)_2$-bpy} (0.115 g, 0.38 mmol) and K_2PtCl_4 (0.13 g, 0.32 mmol) was refluxed in 40 mL of water for 18 h.[22] A bright yellow powder precipitated on cooling. Yield: 70.3%. Anal. Calcd for $C_{16}H_{16}N_2O_4PtCl_2$: C, 33.9; H, 2.8; N, 4.9. Found: C, 34.4; H, 3.2; N 4.7.

(14) Cummings, S. D.; Eisenberg, R. *J. Am. Chem. Soc.* **1996**, *118*, 1949.
(15) Paw, W.; Cummings, S. D.; Mansour, M. A.; Connick, W. B.; Geiger, D. K.; Eisenberg, R. *Coord. Chem. Rev.* **1998**, *171*, 125.
(16) McInnes, E. J. L.; Farley, R. D.; Macgregor, S. A.; Taylor, K. J.; Yellowlees, L. J.; Rowlands, C. C. *J. Chem. Soc., Faraday Trans.* **1998**, *94*, 2985.
(17) Zuleta, J. A.; Burberry, M. S.; Eisenberg, R. *Coord. Chem. Rev.* **1990**, *97*, 47.
(18) Zuleta, J. A.; Bevilacqua, J. M.; Eisenberg, R. *Coord. Chem. Rev.* **1991**, *111*, 237.
(19) Yoo, J.; Kim, J.-H.; Sohn, Y. S.; Do, Y. *Inorg. Chim. Acta* **1997**, *263*, 53.
(20) Xie, P.-H.; Hou, Y.-J.; Wei, T.-X.; Zhang, B.-W.; Cao, Y.; Huang, C.-H. *Inorg. Chim. Acta* **2000**, *308*, 73.
(21) Markl, G.; Vybiral, R. *Tetrahedron Lett.* **1989**, *30*, 2903.
(22) Dholakia, S.; Gillard, R. D.; Wimmer, F. L. *Polyhedron* **1985**, *4*, 791.
(23) Case, F. H. *J. Am. Chem. Soc.* **1946**, *68*, 2574.

Synthesis of [Pt{4,4′(CO$_2$H)$_2$-bpy}Cl$_2$]. [Pt{4,4′(CO$_2$H)$_2$-bpy}Cl$_2$] was synthesized by a previously reported method.[12] Yield: 87.9%. Anal. Calcd for $C_{12}H_8N_2O_4PtCl_2$: C, 28.3; H, 1.6; N, 5.5. Found: C, 28.5; H, 2.0; N, 5.7.

Synthesis of [Pt{4,4′(CO$_2$Et)$_2$-bpy}Cl$_2$]. [Pt{4,4′(CO$_2$Et)$_2$-bpy}Cl$_2$] was synthesized in the same manner as the 3,3′-analogue. Yield: 76.1%. Anal. Calcd for $C_{16}H_{16}N_2O_4PtCl_2$: C, 33.9; H, 2.8; N, 4.9. Found: C, 32.9; H, 2.4; N, 4.9.

Synthesis of [Pt{5,5′(CO$_2$H)$_2$-bpy}Cl$_2$]. [Pt{5,5′(CO$_2$H)$_2$-bpy}Cl$_2$] was synthesized by a previously reported method.[13] Yield: 71.8%. Anal. Calcd for $C_{12}H_8N_2O_4PtCl_2$: C, 28.3; H, 1.6; N, 5.5. Found: C, 28.8; H, 1.7; N, 5.5.

Synthesis of [Pt{5,5′(CO$_2$Et)$_2$-bpy}Cl$_2$]. [Pt{5,5′(CO$_2$Et)$_2$-bpy}Cl$_2$] was synthesized in the same manner as the 3,3′-analogue. Yield: 76.2%. Anal. Calcd for $C_{16}H_{16}N_2O_4PtCl_2$: C, 33.9; H, 2.8; N, 4.9. Found: C, 33.0; H, 2.7; N, 4.8.

Synthesis of [Pt{3,3′(CO$_2$H)$_2$-bpy}(mnt)] (1a). [Pt{3,3′(CO$_2$H)$_2$-bpy}Cl$_2$] (0.80 g, 1.57 mmol) was dissolved in 2 equiv of 1 M aqueous solution of potassium hydroxide under nitrogen, and a solution of Na_2(mnt) (0.44 g, 2.36 mmol) in dry methanol (5 mL) was added. The reaction was allowed to stir at room temperature under N_2 for 48 h. The product was precipitated using 2 equiv of concentrated HCl and filtered. It was subsequently purified by column chromatography using Sephadex-LH20 as a separating medium by a method previously described.[12] Yield: 20.0%. MS (FABMS) *m*/*z*: 580 (M^+). Anal. Calcd for $C_{16}H_8N_4O_4PtS_2$: C, 33.2; H, 1.4; N, 9.7. Found: C, 32.4; H, 1.9; N, 9.0.

Synthesis of [Pt{3,3′(CO$_2$Et)$_2$-bpy}(mnt)] (1b). [Pt{3,3′-(CO$_2$Et)$_2$-bpy}Cl$_2$] (0.47 g, 0.83 mmol) was dissolved in dry acentonitrile under nitrogen and a solution of Na_2(mnt) (0.23 g, 1.24 mmol) in dry methanol (5 mL) was added. The reaction was allowed to stir at room temperature under N_2 for 4 h. The solvent was removed and the product was washed with methanol before recrystallization from acentonitrile. Yield: 22.1%. MS (FABMS) *m*/*z*: 636 (M^+). IR (KBr, cm^{-1}): 1729 (s) (C═O stretch), 2204 (s) (C≡N stretch). Anal. Calcd for $C_{20}H_{16}N_4O_4PtS_2$: C, 37.8; H, 2.5; N, 8.8. Found: C, 37.3; H, 2.5; N, 8.6.

Synthesis of [Pt{4,4′(CO$_2$H)$_2$-bpy}(mnt)] (2a). Compound **2a** was synthesized by an analogous method to compound **1a**. Yield: 28.5%. MS (FABMS) *m*/*z*: 580 (M^+). Anal. Calcd for $C_{16}H_8N_4O_4PtS_2$: C, 33.2; H, 1.4; N, 9.7. Found: C, 32.2; H, 2.1; N 9.0.

Synthesis of [Pt{4,4′(CO$_2$Et)$_2$-bpy}(mnt)] (2b). [Pt{4,4′-(CO$_2$Et)$_2$-bpy}Cl$_2$] (0.14 g, 0.25 mmol) was dissolved in DMF (15 mL) and heated under nitrogen to just below the boiling point (140 °C). A solution of Na_2(mnt) (0.07 g, 0.37 mmol) in dry methanol (5 mL) was added and the reaction mixture was refluxed with stirring under N_2 for 1 h and then allowed to stir under N_2 at room temperature overnight. The solvent was removed and the product was washed with water and methanol before recrystallization from a hot saturated solution of DMF. Yield: 72.0%. MS (FABMS) *m*/*z*: 636 (M^+). IR (KBr, cm^{-1}): 1730 (s) (C═O stretch), 2207 (s) (C≡N stretch). Anal. Calcd for $C_{20}H_{16}N_4O_4PtS_2$: C, 37.8; H, 2.5; N, 8.8. Found: C, 38.0; H, 3.1; N, 8.6.

Synthesis of [Pt{5,5′(CO$_2$H)$_2$-bpy}(mnt)] (3a). Compound **3a** was synthesized by an analogous method to compound **1a**. Yield: 18.0%. MS (FABMS) *m*/*z*: 580 (M^+). Anal. Calcd for $C_{16}H_8N_4O_4PtS_2$: C, 33.2; H, 1.4; N, 9.7. Found: C, 32.1; H, 2.1; N 8.0.

Synthesis of [Pt{5,5′(CO$_2$Et)$_2$-bpy}(mnt)] (3b). [Pt{5,5′(CO$_2$-Et)$_2$-bpy}Cl$_2$] (0.25 g, 0.44 mmol) was suspended in DMSO (15 mL) under nitrogen and a solution of Na_2(mnt) (0.12 g, 0.66 mmol) in dry methanol (5 mL) was added. The reaction was allowed to stir at room temperature under N_2 for 48 h. The solvent was removed and the product was recrystallized from a hot saturated solution of DMF. Yield: 60.0%. MS (FABMS) *m*/*z*: 636 (M^+). IR (KBr, cm^{-1}): 1725 (s) (C═O stretch), 2208 (s) (C≡N stretch). Anal. Calcd for $C_{20}H_{16}N_4O_4PtS_2$: C, 37.8; H, 2.5; N, 8.8. Found: C, 35.6; H, 2.6; N 7.7.

Table 1. Crystallographic Data for 1b

chemical formula	$C_{22}H_{19}N_5O_4PtS_2$	D_c, Mg m^{-3}	1.898
fw	676.65	μ, mm^{-1}	6.140
T, K	150	reflcts collected	21845
lattice type	monoclinic	unique (R_{int})	5694 (0.07)
space group	$P2_1/c$	no. $I > 2\sigma$	3856
a, Å	14.7735(15)	T_{min}/T_{max}	0.217/1.000
b, Å	21.632(2)	parameters	153
c, Å	7.5450(7)	R_1 [$F > 4\sigma(F)$]	0.0665
β, deg	100.815(4)	wR	0.0751
V, Å^3	2368.4(4)	S	1.0402
no. reflns for cell	4515	$\Delta\rho_{max}$/e Å^{-3})	6.91
$2\theta_{max}$ (deg)	50	$\Delta\rho_{min}$/e Å^{-3}	−4.03
Z	4		

X-ray Crystallography. Purple needle-shaped crystals of [Pt{3,3′(CO$_2$Et)$_2$bpy}(mnt)] (**1b**) (dimensions 1.00 × 0.08 × 0.06 mm^3) were grown by recrystallization from a hot saturated solution of **1b** in acetonitrile. Crystal, data collection, and refinement parameters are summarized in Table 1.

Single-crystal X-ray structure determination was carried out using a Smart APEX CCD diffractometer equipped with an Oxford Cryosystems low-temperature device with Mo Kα radiation for data collection. An absorption correction was applied using the multiscan procedure SADABS.[24] The structure was solved by direct methods and refined by full-matrix least squares against |*F*| using data where $I > 2\sigma(I)$.[25] Hydrogen atoms were placed in calculated positions. The platinum and sulfur atoms were refined with anisotropic displacement parameters (adps). Other light atoms (C, N, O) were refined isotropically; adps for these atoms were rather distorted when refined, while not significantly contributing to better data-fitting.

Other Experimental Information. All UV/vis spectra were recorded on a Perkin-Elmer Lambda 9 spectrophotometer controlled by a Datalink PC, running UV/Winlab software.

Electrochemical studies were carried out using a DELL GX110 PC with General Purpose Electrochemical System (GPES), version 4.8, software connected to an autolab system containing a PGSTAT 20 potentiostat. The techniques used a three-electrode configuration, with a 0.5 mm diameter Pt disk working electrode, a Pt rod counter electrode, and an Ag/AgCl (saturated KCl) reference electrode against which the ferrocenium/ferrocene couple was measured to be +0.55 V. The supporting electrolyte was 0.1 M tetrabutylammonium tetrafluoroborate ($TBABF_4$).

OTTLE (optically transparent thin layer electrode) measurements were taken using a quartz cell of 0.5 mm, a Pt/Rh gauze working electrode, an Ag/AgCl reference electrode, and a Pt wire counter electrode.[26] UV/vis spectra were recorded on a Perkin-Elmer Lambda 9 spectrophotometer, controlled by a Datalink PC, running UV/Winlab software. Spectroelectrochemical measurements were carried out on each of compounds **1b**, **2b**, and **3b**. Measurements on all samples were carried out at 213 K in DMF. $TBABF_4$ (0.1 M) was used as the supporting electrolyte in all cases.

Electronic emission spectra were recorded on a Jobin Yvon Spex Fluoromax spectrofluorimeter, connected to a DSC Datalink PC

(24) Sheldrick, G. M. *SADABS. Bruker-AXS* **1997**.
(25) Betteridge, P. W.; Carruthers, J. R.; Cooper, R. I.; Prout, K.; Watkin, D. J. *J. Appl. Crystallogr.* **2003**, *36*, 1487.
(26) McGregor, S. A.; McInnes, E. J. L.; Sorbie, R. J.; Yellowlees, L. J. *Molecular Electrochemistry of Inorganic, Bioinorganic and Organometallic Compounds*; Kluwer: Dordrecht, The Netherlands, 1993; p 503.

Scheme 1. Preparation of Complexes **1a**, **2a**, **3a**, **1b**, **2b**, and **3b**[a]

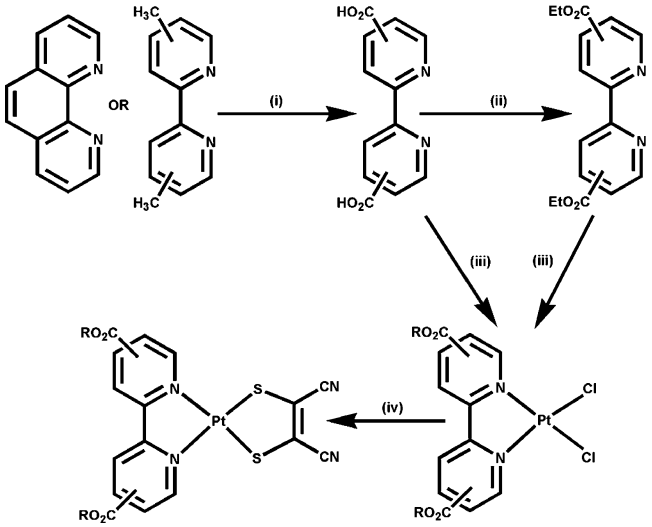

[a] (i) $KMnO_4$(aq), 120 °C/HCl; (ii) EtOH/H_2SO_4, 115 °C; (iii) K_2PtCl_4, 125 °C; (iv) Na_2(mnt), rt (140 °C for **2b**).

running Instruments S. A. Datamax software. All emission spectra were recorded with compounds **1b**, **2b**, and **3b** dissolved in DMSO and dispersed in EtOH. All frozen spectra were recorded in standard Wilmad 5 mm quartz NMR tubes contained in a liquid nitrogen filled fused silica dewar.

Nanoporous TiO_2 thin films (4 μm thick) on FTO conductive glass were prepared as previously reported.[27] The size of all samples was 1 cm^2. The thin films were sensitized at room temperature for 21 h in a 1.7 mM solution of **1a** in DMSO:MeCN (1:1) and a 1.7 mM solution of **2a** and **3a** both in DMSO. Device fabrication was completed as previously described by employing "sandwich type" photovoltaic cells with I^-/I_3^- system electrolyte and a transparent platinized FTO counter electrode. [28] The electrolyte used contained 0.1 M LiI, 0.8 M TBAI, 0.1 M I_2, and 0.5 M ^{t}BuPy in acetonitrile. The working electrode had an illuminated surface area of 1.0 cm^2. Transient absorption studies were carried out as reported previously, employing an excitation wavelength of 540 nm.[27] Photoelectrochemical measurements were conducted under AM 1.5 simulated sunlight as detailed previously.[28]

Results and Discussion

Synthesis and Structure. The [Pt{*X*,*X*′$(CO_2H)_2$-bpy}(mnt)] (*X*,*X*′ = 3,3′, 4,4′, or 5,5′) complexes (**1a**, **2a**, and **3a**) were synthesized by a route analogous to those reported previously.[12,13] The dicarboxylic acid substituted-bpy ligand was made by oxidation of 1,10-phenanthroline to give the 3,3′-dicarboxylic acid product and by oxidation of the 4,4′- and 5,5′-dimethyl-substituted bpy to give the 4,4′- and 5,5′-dicarboxylic acid products, respectively. Reaction of {*X*,*X*′$(CO_2H)_2$-bpy} with potassium tetrachloroplatinate gave the dichloro-substituted platinum precursors [Pt{*X*,*X*′$(CO_2H)_2$-bpy}Cl_2]. Further reaction of these molecules with the disodium salt of mnt gave the desired products **1a**, **2a**, and **3a** (Scheme 1).

Compounds **1b**, **2b**, and **3b** were synthesized to facilitate characterization of the dye molecules, since they are soluble in a greater number of organic solvents, including DMF and acetonitrile. They were synthesized by a method similar to those of compounds **1a**, **2a**, and **3a**. Esterification of {*X*,*X*′$(CO_2H)_2$-bpy} gave {*X*,*X*′$(CO_2Et)_2$-bpy} and refluxing these ligands with potassium tetrachloroplatinate gave the dichloro-substituted platinum precursors [Pt{*X*,*X*′$(CO_2Et)_2$-bpy}Cl_2]. Further reation of these molecules with the disodium salt of mnt gave the desired products **1b**, **2b**, and **3b** (Scheme 1).

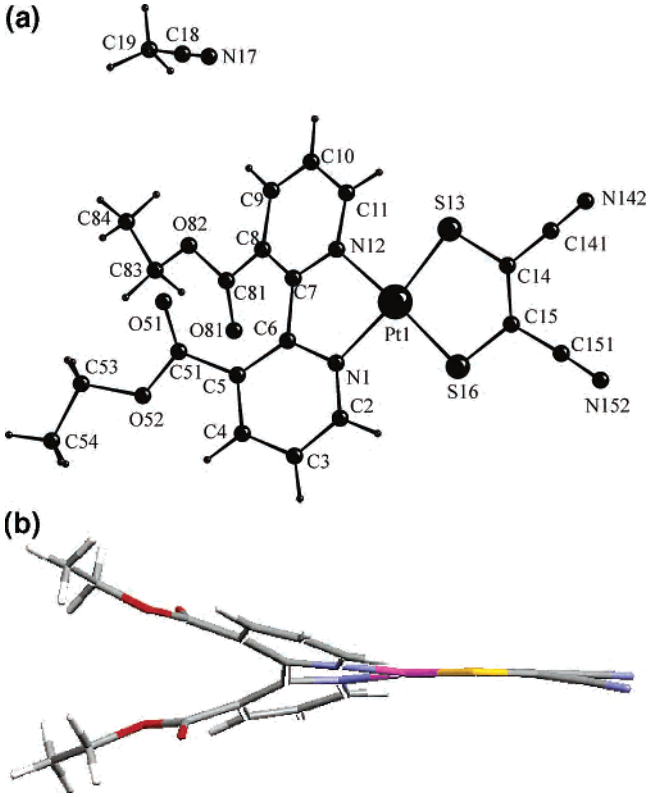

Figure 1. (a) X-ray crystal structure of **1b**. Selected bond lengths (Å) and angles (deg): Pt−S(13), 2.258(2); Pt−S(16), 2.245(3); Pt−N(1), 2.074(10); Pt−N(12), 2.058(8); N(1)−Pt−N(12), 79.4(3); N(12)−Pt−S(13), 96.2(2); S(13)−Pt−S(16), 89.54(9); S(16)−Pt−N(1), 95.3(1). (b) X-ray crystal structure of **1b** with a view down the C═C bond of mnt, showing the large torsion angle induced between the pyridyl rings by the 3,3′CO_2Et substituents. Sulfur atoms are shown in yellow, platinum in pink, carbon in gray, nitrogen in pale blue, oxygen in red, and hydrogen in white.

Only 12 crystal structures of [Pt(bpy)(1,2-dithiolate)] systems have previously been reported.[29] Five of the 12 structures have a 4,4′-disubstituted bpy, one is a 5,5′-disubstituted bpy, and the remaining six feature an unsubstituted bpy. Only 10 structures are known of any complex where Pt is attached to a 3,3′-disubstituted bpy. There have, however, been no previous reports of a crystal structure with a 3,3′-disubstituted bpy in a [Pt(bpy)(dithiolate)] complex. The structure of **1b** shows bond lengths and angles to be similar to those for [Pt(bpy)(dithiolate)] complexes previously reported (Figure 1a).[29] The [Pt(bpy)(dithiolate)] unit shows a 0.0768 Å deviation from planarity. In general, bpy ligands have been seen to retain a planar geometry at square planar Pt centers. Only four of the 12 published [Pt(bpy)(1,2-

(27) Willis, R. L.; Olson, C.; O'Regan, B.; Lutz, T.; Nelson, J.; Durrant, J. R. *J. Phys. Chem. B* **2002**, *106*, 7605.
(28) Palomares, E.; Clifford, J. N.; Haque, S. A.; Lutz, T.; Durrant, J. R. *J. Am. Chem. Soc.* **2003**, *125*, (2), 475.
(29) Cambridge Structural Database. *Chem. Des. Autom. News* **1993**, *8*, 31.

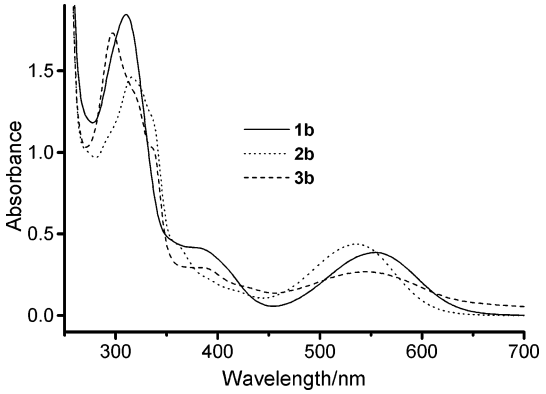

Figure 2. UV/vis spectra of **1b**, **2b**, and **3b** in DMF at 298 K.

Table 2. Absorption Maxima and Molar Extinction Coefficients for Compounds **1b**, **2b**, and **3b** (in Solution of DMF)

compd	λ_{max}/nm (ν/cm^{-1})	ϵ/M^{-1} cm^{-1}
1b	556 (18 000)	4200
2b	537 (18 640)	5600
3b	546 (18 330)	3100

dithiolate)] structures show a bpy torsion angle of greater than 5° and the greatest of these is only 12.7° (in a 4,4′-^{t}Bu$_2$ substituted bpy). Three of these examples occur in 4,4′-^{t}Bu$_2$-substituted bpy ligands and one in an unsubstituted bpy ligand.[30,31] Unsurprisingly, the steric interference between the ethyl chains on the ester substituents of **1b** causes a twist in the pyridine rings with respect to one another. This results in a significant torsion angle of 30.7° between the pyridine rings in the 3,3′-disubstituted bpy moiety, the largest known angle in any [Pt(bpy)(1,2-dithiolate)] complex. This is only slightly smaller than the largest torsion angle of 31.1°, where in a [Pt(bpy)(Cl)$_2$] complex the 3,3′-positions of bpy were substituted with a crown ether.[32] The twisting of the two pyridine rings with respect to each other as seen in the crystal structure may in some part help in the explanation of the interesting electrochemistry of the complex (see Figure 1b). The complex packs in layers with short contacts of 3.488 and 3.810 Å between the sulfur atom on the mnt and the carbonyl oxygen atom from the ester group on the bpy.

UV/Visible Spectroscopy. The UV/vis spectra of compounds **1b**, **2b**, and **3b** in solution show an intense UV band at approximately 300 nm (Figure 2) assigned to the intraligand $\pi-\pi^*$ transition of the diethyl ester-bpy ligand.[14] The charge-transfer band of compounds **1b**, **2b**, and **3b** stretches from 450 to 650 nm with absorbance maxima listed in Table 2. The charge transfer band in [Pt(diimine)(dithiolate)] complexes has previously been assigned by Eisenberg and co-workers. This CT is said to occur from a HOMO consisting of a mixture of Pt(d) and dithiolate(p) orbital character to a low-energy π^* orbital LUMO located on the bpy.[11,14]

(30) Kubo, K.; Nakano, M.; Tamura, H.; Matsubayashi, G.-E. *Inorg. Chim. Acta* **2002**, *336*, 120.
(31) Smucker, B. W.; Hudson, J. M.; Omary, M. A.; Dunbar, K. R. *Inorg. Chem.* **2003**, *42*, 4714.
(32) Gund, A.; Keppler, B. K. *Angew. Chem., Int. Ed. Engl.* **1994**, *33*, 186.
(33) Heath, G. A.; Yellowlees, L. J.; Braterman, P. S. *Chem. Commun.* **1981**, 287.
(34) Coombe, V. T.; Heath, G. A.; MacKenzie, A. J.; Yellowlees, L. J. *Inorg. Chem.* **1984**, *23*, 3423.

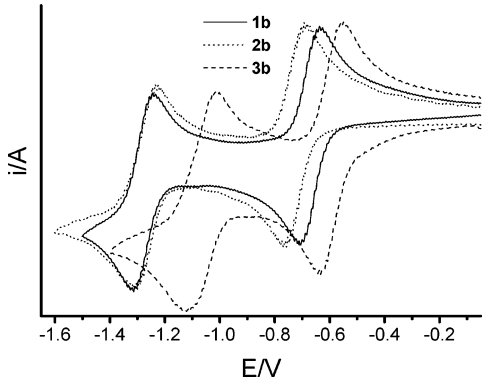

Figure 3. Cyclic voltammogram of **1b**, **2b**, and **3b** showing the two bpy based electrochemically reversible reductions, scan rate 0.1 V s^{-1}, in 0.1 M TBABF$_4$/DMF at 298 K.

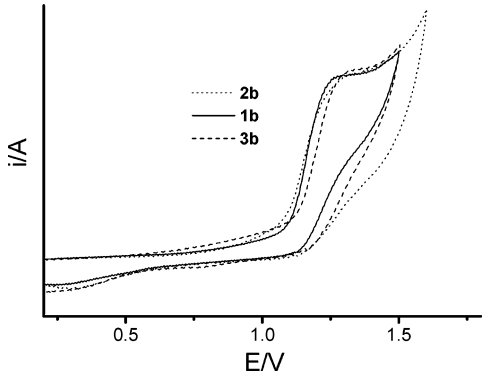

Figure 4. Cyclic voltammogram of **1b**, **2b** and **3b**, showing the partly mnt based irreversible oxidation, scan rate 0.1 V s^{-1}, in 0.1 M TBABF$_4$/DMF at 298 K.

Table 3. Oxidation and Reduction Potentials for Compounds **1a**, **2a**, **3a**, **1b**, **2b**, and **3b** vs Ag/AgCl in Solution of 0.1 M TBABF$_4$/DMF at 298 K

compd	reduction/V		oxidation/V
1a	−1.05[b]	−0.69[b]	+1.27[b]
2a	−1.19[b]	−0.82[b]	+1.27[b]
3a	−1.16[b]	−0.69[b]	+1.27[b]
1b	−1.20[a]	−0.59[a]	+1.35[b]
2b	−1.20[a]	−0.65[a]	+1.39[b]
3b	−0.99[a]	−0.52[a]	+1.41[b]

[a] Peaks are electrochemically reversible and values shown represent $E_{1/2}$. [b] Peaks are electrochemically irreversible and values shown represent peak potential.

Electrochemistry. The electrochemistry of compounds **1b**, **2b**, and **3b** was studied by cyclic voltammetry. All of the scans (in a solution of DMF/0.1 M TBABF$_4$) show two fully reversible reduction peaks (Figure 3), as evidenced by straight line plots of i_{max} vs (scan rate)$^{1/2}$ and one irreversible oxidation peak (Figure 4) (see also Table 3). Previous studies have shown that the diimine ligand influences the reduction potential of the compound and the dithiolate ligand influences the oxidation potential, since the LUMO resides on the bpy and the HOMO is at least partly dithiolate based.[12−14] The oxidation for all three ester dyes occurs at very similar potentials; therefore, this is assigned as the oxidation of the HOMO on the dithiolate moiety. The dithiolate moiety is identical in all three of the complexes; hence, it is expected that these oxidations will occur at similar potentials. Both of the reductions on **3b** occur at the least negative potential

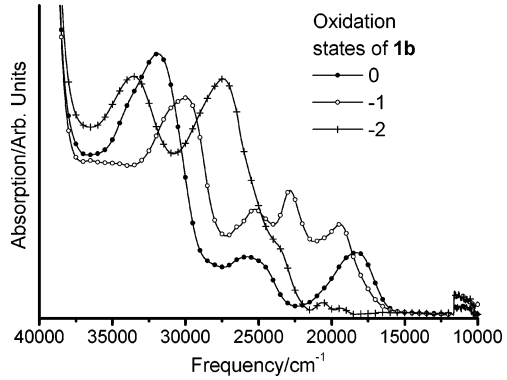

Figure 5. UV/vis/NIR of **1b** in 0, −1, and −2 oxidation states. Spectra were run in 0.1 M $TBABF_4$/DMF at 213 K. E_{gen} = 0 V (0), −1.0 V (−1), −1.6 V (−2).

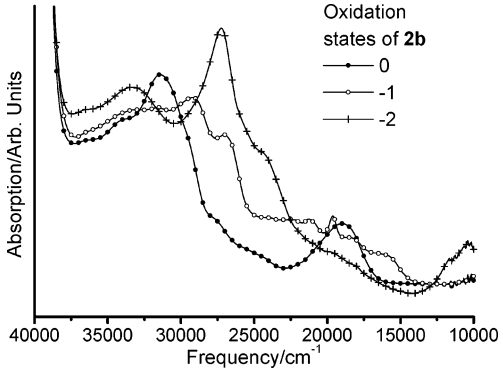

Figure 6. UV/vis/NIR of **2b** in 0, −1, and −2 oxidation states. Spectra were run in 0.1 M $TBABF_4$/DMF at 213 K. E_{gen} = 0 V (0), −1.0 V (−1), −1.6 V (−2).

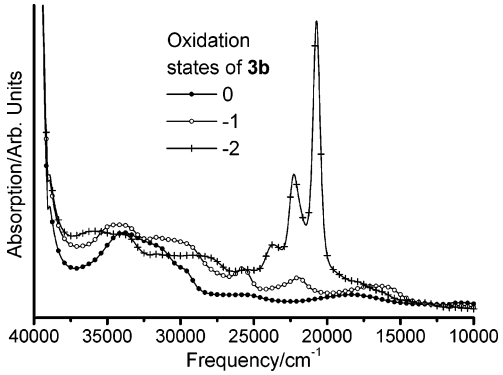

Figure 7. UV/vis/NIR of **3b** in 0, −1, and −2 oxidation states. Spectra were run in 0.1 M $TBABF_4$/DMF at 213 K. E_{gen} = 0 V (0), −0.8 V (−1), −1.3 V (−2).

of the three compounds, consistent with our previous findings.[13] This is due to the more electron withdrawing nature of the 5,5′-position of the bpy ring with respect to its 4,4′- and 3,3′-analogues. The first reduction potential of **1b** occurs at less negative potential than that of **2b**. As the crystal structure of **1b** shows a significant torsion angle (30.7°) between the two pyridine rings of the bpy moiety, this lack of planar character may interfere with the delocalization of charge between the two pyridine rings in the bpy, thus causing it to behave more like two separate pyridine rings than a bpy functionality. Therefore, the electrochemical response of 3,3′-disubstituted bpy is influenced by both electronic and steric effects and this results in its electrochemistry being intermediate between that of the 5,5′- and 4,4′-disubstituted ligands. The cyclic voltammetry of compounds **1a**, **2a**, and **3a** in DMF showed very similar oxidation and reduction potentials to those of **1b**, **2b**, and **3b.** In addition to this, the similarity of the UV/vis spectra of **1b**, **2b**, and **3b** in DMF and those of **1a**, **2a**, and **3a** on TiO_2 enables the data for **1b**, **2b**, and **3b** in solution to be used as models for **1a**, **2a**, and **3a** on TiO_2 (see Table 3).

Spectroelectrochemistry. UV/vis/NIR spectroelectrochemistry was performed to electronically characterize the frontier orbitals of compounds **1b**, **2b**, **and 3b**. This involved electrochemical reduction of **1b**, **2b**, and **3b** to $\mathbf{1b}^{1-}$, $\mathbf{2b}^{1-}$, and $\mathbf{3b}^{1-}$ and also to $\mathbf{1b}^{2-}$, $\mathbf{2b}^{2-}$, and $\mathbf{3b}^{2-}$, respectively. The irreversible nature of the one-electron oxidation process precludes spectroelectrochemical study of the oxidized molecules. Each of the neutral complexes shows a similar spectrum with several diagnostic peaks present (Figures 5−7). Peaks at greater than 30 000 cm^{-1} are assigned as $\pi-\pi^*$ intraligand bpy transitions, as previously reported.[14] In **1b**, **3b**, and as a broad shoulder in **2b**, the absorbance at approximately 26 000 cm^{-1} is assigned as a mainly Pt-based $d-\pi^*$ MLCT. Each of the three neutral compounds shows an absorbance at approximately 19 000 cm^{-1}, which is assigned as MMLL′CT verified by the absence of the peak in each of the corresponding $[Pt\{X,X'(CO_2Et)_2\text{-bpy}\}Cl_2]$ precursors. The three monoreduced species $\mathbf{1b}^{1-}$, $\mathbf{2b}^{1-}$, and $\mathbf{3b}^{1-}$ show similar spectral properties to each other (Figures 5−7). On reduction there is a decrease in the intensity of the $\pi-\pi^*$ absorbance of the bpy ligand above 30 000 cm^{-1}. Furthermore, all three monoreduced species show a multiplet of bands in the visible region. Similar peaks are also observed in the spectra of the related dichloride species $[Pt\{X,X'(CO_2Et)_2\text{-bpy}\}Cl_2]^{1-}$; hence, the reduction electron appears to enter an orbital primarily based on the derivatized bpy ligand, consistent with the results of the electrochemical study. No additional features may be observed that differ between the $[Pt\{X,X'(CO_2Et)_2\text{-bpy}\}Cl_2]^{1-}$ and $[Pt\{X,X'(CO_2Et)_2\text{-bpy}\}(mnt)]^{1-}$ spectra; therefore, the bands in $[Pt\{X,X'(CO_2Et)_2\text{-bpy}\}(mnt)]^{1-}$ complexes may be confidently assigned as intraligand transitions of the monoreduced derivatized bpy ligand.

The spectra of the direduced species $\mathbf{1b}^{2-}$, $\mathbf{2b}^{2-}$, and $\mathbf{3b}^{2-}$ are all very different from the monoreduced species with $\mathbf{1b}^{2-}$ and $\mathbf{2b}^{2-}$ being similar and $\mathbf{3b}^{2-}$ showing a very intense absorption centered at 22 500 cm^{-1}. Once again the spectra are remarkably consistent with those of $[Pt\{X,X'(CO_2Et)_2\text{-bpy}\}Cl_2]^{2-}$, and it can therefore be concluded that the second reduction electron is entering an orbital primarily based on the derivatized bpy ligand. Hence, all bands in the low-energy region of the absorption spectra are assigned to the intraligand transitions of the direduced bpy ligand.

In every case, after recording the final spectra the potential was adjusted so that the neutral starting material was regenerated, and the absorption spectra were observed to return to exactly that of the starting species. Thus, the monoreduced and direduced species are all stable at 213 K.

Luminescence Studies. We observed weak emission from a solution of each of compounds **1b**, **2b**, and **3b** in DMSO

Table 4. Emission and Corresponding Excitation Values for Compounds **1b**, **2b**, and **3b** in Frozen Glass of DMSO Dispersed in EtOH

compd	emission observed (nm) after excitation at 550 nm	excitation peaks (nm) corresponding to emission at tabulated wavelength
1b	655	375, 525, 565
2b	630	345, 420, 555
2b	680	not observed
3b	670	370, 495, 530, 575
3b	735	400−530,[a] 575

[a] Broad band absorbance.

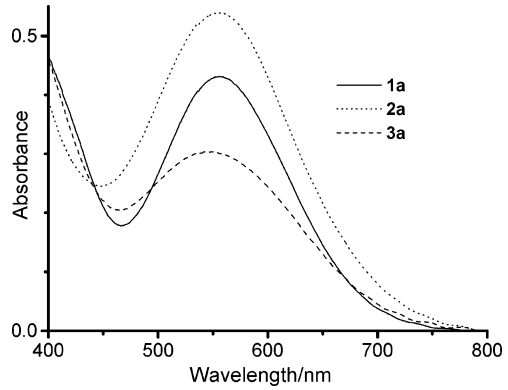

Figure 8. UV/vis measurement for nanoporous TiO_2 sensitized by dyes **1a**, **2a**, and **3a**.

dispersed in EtOH at room temperature. Each of the complexes showed similar emissive properties. Excitation of the complexes at 550 nm gave an emission spectrum with a peak at approximately 700 nm. The corresponding excitation spectra showed a peak at approximately 450 nm. In a frozen solution at 77 K, much stronger emission was observed. The emission and corresponding excitation values for **1b**, **2b**, and **3b** are shown in Table 4. The observed excitation wavelengths correspond largely to those seen in the absorption spectra of **1b**, **2b**, and **3b**, thus confirming **1b**, **2b**, and **3b** to be the emissive species in solution. This observation of emission in fluid solution confirms that the excited-state lifetime of these complexes is long in comparison with the time scale of electron injection into the TiO_2 conduction band. To draw further conclusions from these preliminary results, a more detailed study of the lifetimes of the emitting states involved in the luminescence is currently underway.

Sensitization of Nanocrystalline TiO_2 Films. Immersion of nanocrystalline TiO_2 in 1.7 mM solutions of dyes **1a** (in 1:1 MeCN/DMSO), **2a** (in DMSO), and **3a** (in DMSO) resulted in a strong coloration of the films. UV/visible absorption spectra for the resulting dye sensitized films are shown in Figure 8 and in all cases exhibit similar 540−550 nm absorption maxima to that observed for the solution spectra of **1b**, **2b**, and **3b** (Figure 2).

Dye loadings were determined from these film spectra by assuming the molar extinction coefficients determined in solution. These are summarized in Table 5. It is apparent that approximately monolayer dye coverage is achieved for all three dyes, with differences in film optical density primarily arising from the differences in dye molar extinction coefficient.

Table 5. Summary of Results Obtained for Sensitization of Nanocrystalline TiO_2 Films with **1a**, **2a**, and **3a**

	optical density on TiO_2 films[a]	dye coverage ratio[b]	half-times for recombination decay/s[c]	I_{sc}/mA/cm^2 [d]	V_{oc}/mV[d]	cell efficiency/%[d]
1a	0.43	1.05	3.2×10^{-4}	1.94	540	0.64
2a	0.54	0.98	6.5×10^{-6}	2.49	490	0.63
3a	030	1.01	−	0.68	420	0.14

[a] Optical densities were obtained at a maximum. [b] Dye coverage ratio was the ratio of dye coverage area per TiO_2 surface area. Dye coverage was estimated from UV/vis absorption spectra and the ratio was calculated using 7.73×10^{-15} cm^2 as a dye surface area. [c] The data were estimated from Figure 10. The data for **3a** were less reliable because of small signals. [d] See also Figure 11

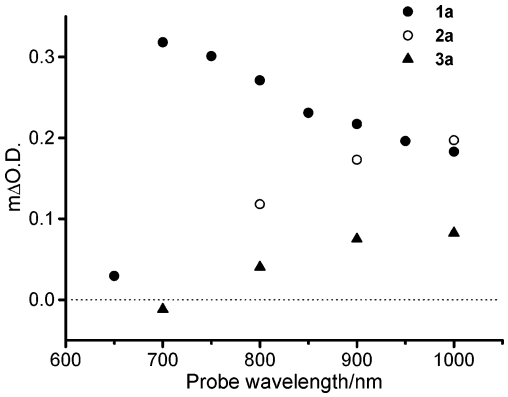

Figure 9. Comparison of the difference absorption spectra of **1a**, **2a**, and **3a** on nanocrystalline TiO_2 film. The spectra were recorded with 550 nm excitation pulse at 10^{-6} s.

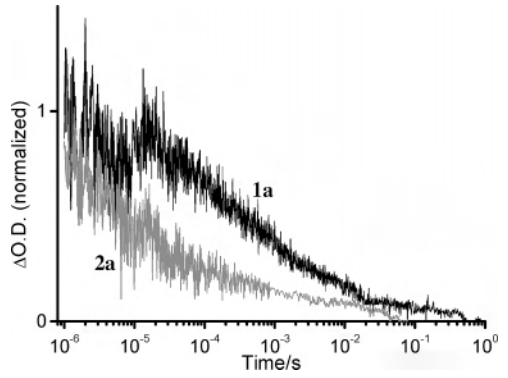

Figure 10. Transient absorption data monitoring the charge recombination kinetics for 4 μm TiO_2 films sensitized with dyes **1a** (black) and **2a** (gray). Experiments employed 550 nm excitation, and all data were collected at 900 nm probe wavelength. The half-life values for dyes **1a** and **2a** are 3.2 $\times 10^{-4}$ and 6.5 $\times 10^{-6}$ s, respectively. The data for **3a** were less reliable because of small signals.

Transient absorption data for the resulting dye-sensitized films covered in organic solvent were obtained following pulsed laser excitation and are shown in Figures 9 and 10. In all cases, a broad absorption increase was observed between 700 and 1000 nm, assigned to induced absorption of the dye cation/$TiO_2(e^-)$ states generated by electron injection from the dye excited state (Figure 9). For **1a**, an absorption maximum was observed at 700 nm and is assigned as dye cation absorption. In contrast, for **2a** and **3a**, the transient spectrum increases steadily toward longer wavelengths, indicating that for these dyes the transient signal is dominated by TiO_2 electron absorption, with cation absorption for these dyes being relatively weak over this spectral

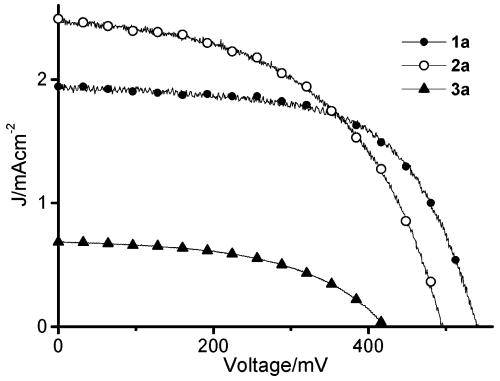

Figure 11. $I-V$ characterization for the liquid DSSC with dyes **1a**, **2a**, and **3a** under 1 sun and AM 1.5 intense illumination. The areas of all samples were 1.0 cm^2. I_{sc}, V_{oc}, ff (fill factor), and efficiency were 1.94 mA, 540 mV, 61.4%, and 0.64% for **1a**; 2.49 mA, 490 mV, 51.3%, and 0.63% for **2a**; 0.68 mA, 420 mV, 50.5%, and 0.14% for **3b**, respectively (see also Table 5).

region. The relatively low signal amplitude for dye **3a** is consistent with the low film optical density due to the low dye molar extinction coefficient.

Decay dynamics of the transient signal, assigned to the recombination of the TiO_2 electrons with dye cations, are shown in Figure 10. Half-times for these decay dynamics are summarized in Table 5. These dynamics are typical of charge recombination dynamics for such dye-sensitized TiO_2 films,[13,30] with dye **2a** showing faster, more dispersive recombination dynamics relative to dye **1a**.

Typical current/voltage characteristics for photoelectrochemical cells sensitized with dyes **1a**, **2a** and **3a** are shown in Figure 11, with the corresponding device efficiencies given in Table 5. It is apparent that there is a good correlation between the UV/visible absorbance data, the transient aborption data, and the device current/voltage characteristics. **2a**, which has the highest optical density, also has the highest short circuit current (I_{sc}), while **1a** exhibits the slowest recombination dynamics and the highest open circuit voltage (V_{oc}).

From the data detailed above, it is apparent that **1a** exhibits the highest photovoltaic device performance of the dye series studied. This device efficiency, however, remains relatively low compared to the more established sensitizer dye, the ditetrabutylammonium salt of $[RuL_2(NCS)_2]$ (L = 2,2′-bipyridyl-4,4′-dicarboxylato), commonly called N719. This lower device efficiency can be primarily attributed to the relatively low optical absorbance of **1a** compared to $[RuL_2(NCS)_2]$ (with peak molar extinction coefficients in the visible of 5615 and 14 000 M^{-1} cm^{-1}, respectively). As the devices presented here employed 4 μm, nonscattering TiO_2 films, this lower optical absorbance can be expected to have a strong effect on device performance. A significant improvement in device performance for **1a** can be expected by the use of thicker TiO_2 films with the addition of light scattering layers. A more detailed characterization of the photovoltaic performance and transient kinetics of devices employing **1a** was undertaken to elucidate whether differences in device performance between **1a** and N719 can be attributed to dye optical absorbance alone or whether other

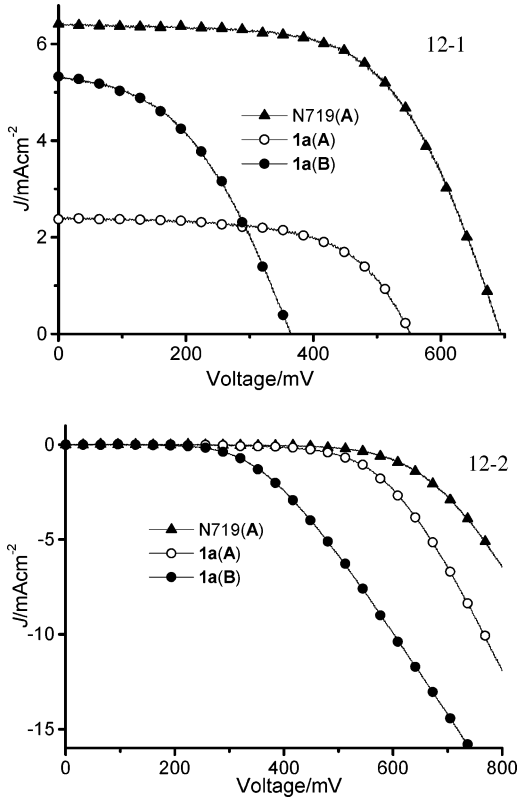

Figure 12. Comparison in terms of cell performance between the cell using electrolyte A (containing *tert*-butyl pyridine (t-BP)) and electrolyte B (without *tert*-butyl pyridine) in the electrolyte. Graph 12-1 represents $I-V$ curve of all three cells under 1 sun illumination. The cell performance, I_{sc}, V_{oc}, ff, and efficiency, were 2.37 mA, 550 mV, 61.5%, and 0.80% for **1a** using electrolyte A; 5.33 mA, 370 mV, 43.6%, and 0.84% for **1a** using electrolyte B; 6.41 mA, 700 mV, 60.4%, and 2.69% for N719 using electrolyte A, respectively. Graph 12-2 shows the data collected under dark conditions.

parameters also limit device performance. Figure 12 shows current/voltage data for **1a**/TiO_2 solar cells employing both the standard electrolyte A (containing the additive *tert*-butyl pyridine (t-BP)), as employed in Figure 9, and an alternative electrolyte B, in which the t-BP was omitted from the electrolyte. Control data employing the N719 dye are also shown for comparison, with the dye loading of N719 being selected to give the same peak optical density as that of **1a** (OD = 0.5 at 535 nm).

Figure 13 shows the corresponding transient absorption signals, with the excitation wavelength of 540 nm corresponding to that at which the optical density of the N719- and **1a**-sensitized devices are identical. Note that these transient data were collected for complete devices rather than for dye-sensitized films alone, as employed in Figure 9, with the probe wavelength of 1000 nm being selected to correspond primarily to absorption of electrons injected into the TiO_2 by the optical laser pulse. It is apparent that for **1a** the omission of t-BP from the electrolyte results in a significantly higher current density, but at the expense of a lower cell voltage. This observation is correlated with a larger transient signal, assigned to long-lived I_2^- product states. This effect is attributed to the established influence of t-BP on the TiO_2 conduction band energetics; the absence of t-BP lowers the TiO_2 conduction band, favoring electron injection and

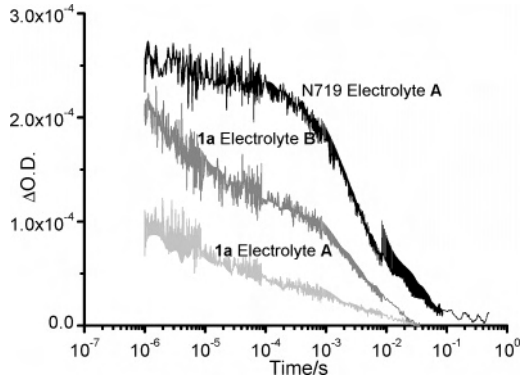

Figure 13. Transient absorption data monitoring charge recombination dynamics following optical excitation at 540 nm. White light was used as a probe light, and all signals were detected at 1000 nm. A comparison in terms of transient absorption decay between the cells with and without t-BP in the electrolyte suggests its effect on the LUMO energy level of the dyes. The N719 cell with t-BP was used as a control cell.

resulting in both the larger transient signal and higher short circuit current. The absence of efficient electron injection for dye **1a** in the presence of t-BP is attributed to the lower dye excited-state oxidation potential relative to N719 (770 mV vs SCE). Strikingly, in the absence of t-BP, both the short circuit current density and transient signal amplitude obtained with **1a** are of similar magnitude to those observed for the control data for N719**.** These data are therefore indicative that, in the absence of t-BP, the quantum efficiencies of both electron injection and dye regeneration for the **1a**/TiO_2 system are near unity.

The lower device voltage obtained with sensitizer **1a** relative to N719 is correlated with the higher dark current associated with this dye. This effect may be associated with the influence of the sensitizer dye on the TiO_2 conduction band energetics. Alternatively, this effect may result from an acceleration of the rate constant for electron recombination with the redox electrolyte. Experiments to further address this point are in progress.

Conclusions

This work has provided us with valuable structural and electronic information for the family of [Pt{*X*,*X*′(CO_2R)$_2$-bpy}(mnt)] complexes. The large torsion angle of **1b** seen in the crystal structure is reflected in the electrochemistry of the complex, thus showing the influence of twisting the bipyridyl rings on the reduction potential of the complexes. The spectroelectrochemical study shows that for all three complexes the reduction electron must be localized on the derivatized bpy moiety of the molecule. This reconfirms previous reports that the LUMO is mainly localized on the bpy. This is the first report of a Pt-based dye sensitizer where the bpy has been substituted in the 3,3′-positions. Interestingly, it shows the best performance of the three sensitizers tested. This result is significant when compared to previous work done in the field, being in sharp contrast with the only report of a Ru sensitizer with a 3,3′-disubstituted bpy, which showed an inferior performance to that of its 4,4′-analogue. The work reported in this paper demonstrates the worth of looking at other anchor ligands in the rational design of solar cell dyes and broadens the scope for further investigations into potential dyes for use in DSSC.

Acknowledgment. We thank Donald Robertson for providing us with the Na_2(mnt) used in this study. Financial support from the EPSRC is gratefully acknowledged.

Supporting Information Available: Crystallographic data for **1b**. This material is available free of charge via the Internet http://pubs.acs.org.

IC048799T